



Materials
Horizons

Enhanced and Unconventional Responses in Chemiresistive Sensing Devices for Nitrogen Dioxide and Ammonia from Carboxylated Alkylthiophene Polymers

Journal:	<i>Materials Horizons</i>
Manuscript ID	MH-COM-01-2020-000049
Article Type:	Communication
Date Submitted by the Author:	09-Jan-2020
Complete List of Authors:	Wagner, Justine; Johns Hopkins University, Materials Science and Engineering Jang, Hyun-June; Johns Hopkins University, Materials Science and Engineering Han, Jinfeng; Johns Hopkins University, Materials Science and Engineering Katz, Howard; Johns Hopkins University, Materials Science and Engineering

SCHOLARONE™
Manuscripts

Enhanced and Unconventional Responses in Chemiresistive Sensing Devices for Nitrogen Dioxide and Ammonia from Carboxylated Alkylthiophene Polymers

Justine Wagner, Hyun-June Jang, Jinfeng Han, Howard E. Katz*

Department of Materials Science and Engineering, Johns Hopkins University, 3400 N. Charles St., Baltimore, USA

New Concepts

Conductances of organic and conjugated polymer semiconductor-based devices can change in response to gas-phase molecules, functioning as detectors thereof. Conductance increases (10-100%/ppm) and decreases (10-90%/ppm) are typical, for dopants or trapping agents, respectively. Larger/opposite responses are rare, and their origins are often not considered. We report three “new concepts” in this field: (1) incorporation of carboxylic acid groups (COOH) in a p-type alkylthiophene polymer results in 1-2 orders-of-magnitude increased NO₂-induced current compared to non-COOH analogues; (2) COOH also gave increased response to NH₃, again as a *current increase, counter to expectations and prior observations* for p-type semiconductors; and (3) the origin of responses to NO₂ is a doping interaction between the NO₂ and polymer observable as an electrochemical potential applied to a coupled silicon transistor, with an added, distinct contribution from another mechanism, likely proton transport, in the COOH polymer. This is the *first direct correlation between increased molecule-induced polymer conductance and independently-measured induced charge*. This mechanism is not observed for NH₃, which is correspondingly not a dopant. We calculated a charge density for the NO₂-exposed COOH polymer far beyond the hole density that could be supported therein, evidence for the proton conduction contribution.

Enhanced and Unconventional Responses in Chemiresistive Sensing Devices for Nitrogen Dioxide and Ammonia from Carboxylated Alkylthiophene Polymers

Justine Wagner¹, Hyun-June Jang¹, Jinfeng Han¹, Howard E. Katz*¹

¹Department of Materials Science and Engineering, Johns Hopkins University, 3400 N. Charles St., Baltimore, USA

◆ Abstract

A carboxylated thiophene polymer-based chemiresistive device in a field-effect transistor (FET) configuration with unusual and enhanced responses to the widespread pollutants nitrogen dioxide (NO₂) and ammonia (NH₃) is described. The device based on a polymeric thiophene carboxylic acid showed a dramatic and superlinear increase in drain current (I_D) of over 15,000% to a ramped exposure to 10 ppm NO₂ over several minutes, while its ethyl ester counterpart had significantly lower response. Devices incorporating either an ester or carboxylic acid displayed comparable and previously unreported increases in I_D from 10 ppm ramped NH₃ exposure of 200-300%. Conventional poly(alkylthiophenes) showed the expected current decreases from similar NH₃ exposures. Using threshold voltage shifts in silicon transistors coupled to our recently reported remote gate (RG) platform with thiophene polymer coatings, we determined that two differing response mechanisms are associated with the two gas exposures. By calculating the charge density induced in the polymers by NO₂ exposure using the silicon transistor voltage shifts, we conclude that proton conduction contributes significantly to the high sensitivity of the carboxylic acid to NO₂, in addition to doping that was observed for all four polymers. Furthermore, hydrogen bonding moieties of the carboxylic acid and ester may be able to physisorb NH₃ and thus alter the charge distribution, rearrange polymer chains, and/or create a proton transfer network leading to the I_D increase that is the opposite of the response obtained from non-carboxylated thiophene polymers.

◆ Introduction

Emissions of chemical pollutants that originate from refining, manufacturing, agriculture and fuel combustion has led to increasing global environmental concerns ranging from acid rain production, the greenhouse effect, and ozone depletion; as well as health concerns.¹⁻⁵ Gases such as nitrogen dioxide (NO₂) and ammonia (NH₃) have garnered specific interest. NO₂ is predominately of interest in the automotive industry and air quality monitoring due to modern diesel engines operating at high air to fuel ratio that results in large NO and NO₂ production.⁶⁻⁸ NH₃ monitoring can be implemented to detect leaks during NH₃ production, exhaust gases can be monitored for pollution in urban areas and “NH₃ slip” in automotive applications, and it can be measured as a component of exhaled air in medical diagnostic applications.⁹⁻¹⁷

Techniques such as gas chromatography, optical spectrometry, colorimetry, chemiluminescence, and electrochemistry have been exploited as detection methods for NO₂¹⁸⁻¹⁹ and NH₃ gas¹⁹⁻²⁵; however, even though selectivity and sensitivity of these approaches are considerable, there are noticeable limitations which exists such as size and expense of

instruments, lack of portability, tedious usage and assembly, challenge in sample preparation, and time duration in data acquisition.

Electronic sensors that generate an electrical output signal can be advantageous because of their high portability, simple operation, and fast response. There are two main configurational arrangements of organic electrical sensors: chemiresistor and organic field-effect transistors (OFETs). Chemiresistor sensors exhibit a change in resistance toward gas analyte exposure where the resistance is proportional to the analyte concentration. There have been recent reports on the usage of the chemiresistor configuration. For example, Zhou et al²⁶ reported polysquaramide based chemiresistors that were able to detect NH₃ with an impressive LOD of 10 parts-per-trillion (ppt) as well as nitric oxide as low as 20 ppb with a fast response/recovery, selectivity, and stability due to its dual hydrogen bonding moiety. In addition, the exploration of an ionic activated sensing mechanism has also been developed where authors have reported that when hydroxide is formed on SnO₂ in the presence of humidity it leads to 132 ppt detection of NO₂ and fast recovery at under 30 seconds.²⁷ An ion-in-conjugation polymer p-polyphenyl squaraine (p-PPS) was designed and fabricated as an NO₂ chemiresistor which displayed high sensitivity at 100 ppb and lowest detection limit of 40 ppt among all reported chemiresistors.²⁸ However, OFET sensors are attractive due to their ability to deliver multi-parameter response which consists of parameters such as charge carrier mobility, threshold voltage, on/off current device, and bulk conductivity of semiconducting film. Charge carrier mobility alone is important in the sense that it relates to the signal transfer speed.²⁹ For chemiresistors, the low signal to noise ratio upon miniaturization depends on the sensing area.³⁰ Lastly, OFETs have variable resistance, the magnitude of which can be adjusted through the modulation of the gate voltage. This constitutes a means of incorporating them into logic circuits.³¹

OFETs have generated widespread interest and have already been successfully evaluated and implemented in NO₂ and NH₃ sensing. A review by Aifeng Lv et al²⁹ summarizes the sensing polymer semiconductors and key parameters of the OFET sensors including analyte sensitivity and response time. Although, chemiresistor configuration have indeed displayed impressive sensitivity, LOD, and response/recovery performance, OFET devices are more ideal and with further fine-tuning and optimization they can possibly exceed organic chemiresistor performances. There has been little evaluation or indication of the mechanism associated with the chemical interaction leading to OFET vapor sensing. Implementation of polymers with polar functional group moieties can help control selectivity and enhance sensitivity. Taking one functional group example, there have been recent reports that demonstrated use of carboxylic acid groups in dipyrrolopyrrole (DPP)-bithiophene conjugated OFET polymers,³² and carboxylic acid-functionalized single-walled carbon nanotubes were employed in order to maximize surface area to volume ratio.³³ However, incorporating highly polar side chains can be challenging because of poor solubility of the polymer making film fabrication difficult, electronic instability of the functionalized polymer, and unreliable synthetic/purification sequences.

In this paper, we report a polymer-based chemiresistive sensor in an FET configuration for NO₂ and NH₃ detection with remarkably high response to incremental exposures. We employed conjugated thiophene polymers with carboxylic acid and ester terminal side chains. The results reveal that the sensing layer comprising an ordinary spin-coated film with the carboxylic acid side chain can sense experimentally delivered NO₂ down to 260 ppb (v/v) and NH₃ down to 180 ppb (v/v) with detectable variation of drain current (I_D) after exposure to NO₂- and NH₃- containing air for just 3 minutes. In addition, incorporating the ester terminal side chain resulted in a high comparable sensitivity to NH₃ as well with NO₂ sensitivity being lower

than that of the carboxylic acid counterpart. All responses resulted in conductance increasing, which for the case of NH_3 appears unprecedented. For comparison, the conventional thiophene polymers poly(3-hexylthiophene) (P3HT) and poly(didodecylquaterthiophene) (PQT12) showed the typical conductance increase response to NO_2 and decrease with NH_3 . The carboxylated polymer responses were superlinear, increasing as a power of gas concentration over 0.5-1.5 ppm. We also utilized a new technique to elucidate the general mechanism and associated reasoning behind the polymer sensing layers' responses to the gas exposures. Incorporating our recently described remote gate (RG) detection platform, we confirm that NO_2 and NH_3 exhibit different interaction mechanisms where NO_2 involves a demonstrated doping behavior which increases the current flowing in the device channel due to the increase in the hole concentration, with likely additional proton conduction in the carboxylic acid polymer. Furthermore, the high sensitivity and unexpected NH_3 response sign of the carboxylic acid and ester polymers were attributed to multiple possible interactions involving protons in the system.

◆ Experimental Section

Materials and Characterization Techniques

Unless otherwise specified, all chemicals were used as purchased without further purification. Solvents used for workups and cleaning were reagent grade and used as received. Poly[3-(3-carboxypropyl)thiophene-2,5-diyl]regioregular (PT-COOH) and poly[3-(3-buanoate)thiophene-2,5-diyl]regioregular (PT-COOR) were purchased from Rieke Metals. The PT-COOR was repurified by Soxhlet extractions with methanol for 24 hours followed by hexanes for 24 hours. Poly(3,3''-didodecyl quarter thiophene) (PQT12) was purchased from Solaris Chem Inc. Poly(3-hexylthiophene-2,5-diyl)regioregular (P3HT) was synthesized in house and the synthesis and purification are outlined in the supporting information.

^1H NMR spectra were measured on a Bruker Avance 300 MHz Spectrometer and chemical shifts are reported in parts per million (ppm). Spectra were recorded in either CDCl_3 or $\text{DMSO-}d_6$. Gel permeation chromatography (GPC) analysis was performed on synthesized P3HT in order to determine molecular weight. The analysis was performed on a Tosoh Bioscience EcoSEC GPC workstation using THF as the eluent (0.35 mL min^{-1} , 40°C through a TSKgel SuperMultipore HZ-M guard column (4.6 mm ID x 2.0 cm, $4 \mu\text{m}$, Tosoh Bioscience). Polystyrene standard (EasiVial PS-M, Agilent) was used to build a calibration curve. P3HT polymer was dissolved in THF (2 mg mL^{-1}), filtered (Millex-FG Syringe Filter Unit, $0.20 \mu\text{m}$, PTFE, EMD Millipore) and injected using an auto-sampler ($10 \mu\text{L}$). GPC analysis could not be performed on PT-COOH and PT-COOR due to the insolubility of the polymers in THF at room temperature. PQT12 had a manufacturer-designated molecular weight of 30,000-80,000.

Surface analysis of polymer thin films was accomplished using a Phi 5600 XPS (15 kV, 300 W, chamber pressure centered at 5.5×10^{-8} Torr) equipped with a Mg $\text{K}\alpha$ X-ray (1253.6 eV) source detected at 1 eV step with a passive energy of 58.7 eV for the full surface scan. For high resolution scans centered on the carbon, oxygen, and sulfur peaks, the step was reduced to 0.25 eV per step size. For XPS analysis, $0.50 \times 0.50 \text{ Si/SiO}_2$ substrate with spin-coated polymer film on the top oxide surface was secured to sample stubs with double sided copper tape. Calibration of the XPS to the C (1s) peak occurred with adjustment of the C (1s) peak centered to

284.5 eV and baseline correction was carried out with CasaXPS software. A Filmetrics F20-NIR, thin film analyzer was used to measure the thickness of the semiconductor thin film on a borosilicate glass slide, in which all thin films were measured as 20 ± 5 nm.

NO₂ (49 ppm molar concentration) balanced with nitrogen and NH₃ (51 ppm) balanced with nitrogen were purchased from Praxair. The air/gas mixture with various concentrations was introduced into a homemade gas flow test chamber by an Environics 4040 series gas dilution instrument. The air itself was purified by going through a series of purification stages of silica gel, carbon black, deoxy-catalyst, and followed by purafil in order to obtain clean air with minimum contamination of other gases that may hinder or alter measurements. The devices were exposed to each subset of gas concentrations for a total of 3 minutes before measuring. The time duration between gas exposure and separate probe station measurement, when used, was <1 minute. These diluted gases were further diluted before sample measurement, and exhausted into a well-ventilated open space to avoid reaching exposure limits for these toxic gases. Field effect characteristics of the devices were determined using a KeySight 1500A Semiconductor Device Analyzer. The mobility of the OFETs in the saturation regime was extracted from the following equation:

$$I_D = \frac{W}{2L} \cdot \mu \cdot C_i \cdot (V_G - V_{TH})^2;$$

where I_D is the drain current that is collected; L and W are the channel length and width, respectively; μ is the mobility of the OFET; C_i is the gate capacitance per unit area; V_G is the gate voltage applied, and V_{TH} is the threshold voltage. The V_{TH} of the device was determined by extrapolating the intercept of the x-axis of the $(I_{D, sat})^{1/2}$ vs V_G plot. All measurements were measured in ambient environment conditions.

Conductivity measurements were performed by using a four-point probe measurement method with an Agilent 4155C Semiconductor Parameter Analyzer. At least six measurements of resistance were measured on each sample surface. The same positions were remeasured when exposing the surface to gas for a time duration of 20 minutes.

Fabrication of Devices

As depicted in Scheme 1, the schematic architecture of the gas sensing device is based on a bottom-gate, top-contact OFET structure with a semiconducting polymer serving as the organic active layer. The OFET was fabricated according to the process outlined below. A heavily doped p-type Si wafer and a layer of dry oxidized SiO₂ (300 nm) were used as a gate electrode and gate dielectric layer, respectively. The wafer was successively cleaned in an ultrasonicated bath with isopropanol and distilled water for 15 minutes each. These substrates were then further purified by immersion in a piranha solution (2:1 mixture of sulfuric acid and 30% hydrogen peroxide - CAUTION-STRONGLY OXIDIZING AND CORROSIVE!) for at least 4 hours. This was followed by rinsing with distilled water and drying under nitrogen flow. For the active organic layer consisting of either our synthesized P3HT, commercial poly[3-(3-carboxypropyl)thiophene-2,5-diyl]regioregular, or commercial poly[3-(Ethyl-4-4-butanoate)thiophene-2,5-diyl]regioregular, the wafer was subjected to ultraviolet-ozone exposure for 30 minutes. For the OFET consisting of commercial PQT12, after piranha treatment, the

substrates were further cleaned in an ultrasonicated bath with isopropanol and hexanes for 15 minutes each, baked at 100°C for 20 minutes, and the surface was modified with hexamethyldisilazane (HMDS). After these steps, the substrates were cleaned with hexanes and isopropanol ultrasonication 15 minutes each, respectively. The stock solutions of the polymers were made by dissolving P3HT (20 mg mL⁻¹), PT-COOR (10 mg mL⁻¹), or PQT12 (10 mg mL⁻¹) in anhydrous chlorobenzene. The solutions were then subjected to ultrasonication for 1 hour before placing on a hot bath at 60°C for additional hour. When cooling to room temperature, the polymer solutions were filtered using a hydrophobic PTFE 0.45 μm membrane. The PT-COOH polymer was dissolved in anhydrous DMF (10 mg mL⁻¹), subjected to ultrasonication for 1 hr, and placed on a hot bath at 60°C for 1 hr before increasing the temperature to 120°C for 15 minutes and removing the solution to cool at room temperature. The solution was then filtered using a hydrophilic PTFE 0.45 μm membrane. The PT-COOR, P3HT, and PQT12 polymer solutions were deposited onto the respective clean wafer substrates outlined above via a 1-step spincoating process at 1600 rpm for 60 seconds, while PT-COOH was deposited at 1600 rpm for 320 seconds. The substrates coated with the thin organic films were all baked at 60°C overnight in a glovebox in order to outgas any residual solvent present. Film thicknesses were measured with a Filmetrics F20-NIR, thin film analyzer. Finally, the OFET was completed by the addition of the source and drain electrodes through the deposition of 50 nm of gold via thermal evaporation using a shadow mask. The length and width of the active channel were 200 μm and 8 mm, respectively. The evaporation rate was maintained between 0.3-0.4 Å/s under a chamber pressure of 3 x 10⁻³ Pa.

Silicon FET Detection using Remote Gate

The RG active film was processed similarly to the above without the addition of the deposited gold source and drain electrodes. The polymer solutions were each individually deposited onto their own respective 1 in x 1 in Si/SiO₂ (300 nm oxide growth) substrates. After thoroughly outgassing overnight at 60°C on a hot plate, the substrates with polymers deposited on them were diced into 1 in x 0.5 in slices. The FET detection system platform is divided into two components: a commercial Si FET (CD4007UB) and a RG module. A scratch was made in order to expose the Si surface on the polymer/SiO₂/Si substrate and the exposed Si is used as the electrode and electrically coupled to the gate of the FET. A drop (20 μL) of acetonitrile (ACN) was placed as the contact between the thin film surface and a dual Ag/AgCl (saturated KCl) reference electrode in order to apply a gate bias. Scheme 2 in **SI** displays a visual illustration. The surface potential variation on the RG module would transfer to the commercial FET and induce a horizontal shift of the transfer curve (V_{TH} shift) that is measured. A shift toward depletion, making the n-FET easier to turn on, would correspond to increased positive potential on the RG. Before exposure to the designated gas concentration, the surface potential was equilibrated between the RG and FET using ACN which would eventually reach a stabilization point where successive scans would overlay and obtain a finalized V_{TH} . The solvent drop was then removed, and the RG modules were exposed to 1 ppm NO₂ or NH₃ for 20 minutes, reconnected to the FET platform, had the drop reapplied, and remeasured for 20 consecutive scans in order to analyze drift and restoration. The procedure was repeated with 20 ppm NO₂ exposure. In order to evaluate recovery and restoration of initial V_{TH} , the remote gate substrates were subjected to a vacuum oven set at 60°C for 1 hr. The same process outlined above occurred with a pristine sample that would be subjected to NH₃ exposure.

◆ Results and Discussion

XPS Characterization

It is expected that three chemically different carbon species should contribute to XPS spectra of all four polymer sensing layers: C-C bonded carbon which represents the alkyl portion and C=C bond with the C-S bond contributing to the thiophene ring. For PT-COOH and PT-COOR, an additional carbon species, the O-C=O representing the distinct carbonyl terminal tail, should be present.

The core level spectra of C 1s, S 2p, and O 1s for pristine PT-COOH, PT-COOR, P3HT, and PQT12 are shown in Figure S1 and S2. The carbon 1s (S1 a,d and S2 a,c) signal consists of a single broad peak with the maximum centered at 286 eV due to charging; however, the peak was re-centered at 284.5 eV to which all other signals were adjusted proportionally. The sulfur 2p (S1 c,f and S2 b,d) signal consists of a single doublet which occurs due to spin-orbit coupling which comprises of the $2p_{1/2}$ and $2p_{3/2}$ splitting.³⁴⁻³⁵ However, all peaks are consistently centered at 164 eV. The polymer sensing layers were prepared under ex situ conditions and exposed to ambient atmosphere during transport from ambient state to vacuum, therefore a slight trace in the presence of native unbonded oxygen which we can see in the full scan of P3HT (Figure S3 C) would be expected. For the PT-COOR and PT-COOH sensing layers, a strong sharp signal for the O 1s core level spectra, which we do see at 532 eV (Figures S1 b,e) and is indicative of the O-C=O bonding, is also as expected. Moreover, the energy width of O 1s core level peak is narrow with a full width at half maximum of about 1.75 eV for PT-COOR compared to the broad peak for PT-COOH with a full width at half maximum of about 3 eV. XPS alone cannot distinguish the exact functionality associated with any given sub-peak; however, we believe the O 1s peak in PT-COOH is much broader compared to PT-COOR due to the presence of intramolecular hydrogen bonding.³⁶⁻³⁹

The full XPS scan (Figure S3) detects all required elements in the composition for each polymer sensing layer with no observable additional elements of concern which would indicate contamination, especially trace metal from polymerization reagents.

Electrical Semiconductor Characterization

We studied the FET characteristics of the polymers using a bottom-gate, top-contact device configuration (Scheme 1). The polymers were deposited onto a p-doped silicon wafer with 300 nm of grown thermal oxide. All polymers were deposited by spin-coating, and gold electrodes acting as the source and drain were vapor-deposited.

Multiple room temperature current-voltage (I-V) characteristics, also known as transfer curves, of PT-COOH, PT-COOR, P3HT, and PQT12 based FETs under ambient conditions, with no intentional gas exposure or light exposure, are shown in Figure 1 a-d. Note that the carboxyl polymers showed only a weak field effect, with about 10% current increase over the applied range of 20 V to -50 V. While this field effect was useful for characterization purposes, the carboxyl polymer devices function essentially as chemiresistors when tested as sensors. The poly(alkylthiophenes) showed conventional transfer characteristics. The characteristics were consecutively measured for 25 scans in order to analyze the ambient environmental drift. PT-COOH, PT-COOR, and P3HT increase in current and show a 5%, 7%, and 3% drift for the first ten scans. However, it is important to point out that the drift between consecutive measurements

decreases with each scan relative to the preceding scan. PQT12, on the other hand, shows decreases in current and 14% drift through the first ten scans. I_{on} and I_{off} are the values of I_{D} when $V_{\text{G}} = -60$ and 0 V, respectively. Based on this compilation, the specific parameters of the devices are compiled and compared in Table S1. It should be understood that the values for the carboxylated polymers are only order-of-magnitude estimates as they cannot be assumed to have reached a “saturation” regime, although for PT-COOR, mobility calculated independently following NO_2 exposure agrees within a factor of two, as discussed later. The V_{T} has a very large positive shift for PT-COOH compared to P3HT which may be partially due to more negative surface potential at the interface between Si/SiO₂ and the interfacial conjugated polymer chains from ionized COOH groups that would attract more holes to the channel.⁴⁰

Figure 1 e-h displays the output characteristics under ambient condition, including the transfer characteristic points at $V_{\text{D}} = -50$ V. It can be clearly seen that P3HT and PQT12 exhibit typical p-channel behavior. However, for PT-COOH and PT-COOR, it can be again observed that the I_{D} displays weak-field effect transistor behavior. The FET carrier mobility was calculated to be $2.3 \times 10^{-2} \pm 8 \times 10^{-3} \text{ cm}^2/\text{V}\cdot\text{s}$, $1.2 \times 10^{-2} \pm 6 \times 10^{-3} \text{ cm}^2/\text{V}\cdot\text{s}$, $1.8 \times 10^{-4} \pm 7 \times 10^{-5} \text{ cm}^2/\text{V}\cdot\text{s}$, and $5.4 \times 10^{-4} \pm 2 \times 10^{-4} \text{ cm}^2/\text{V}\cdot\text{s}$, for PT-COOH, PT-COOR, P3HT, and PQT12, respectively, using the saturation regime currents (or currents at highest V_{D}) and V_{TH} at the intersection of the linear portion of the \sqrt{I} vs V_{G} plots with the x-axis. Five devices were measured and averaged to obtain these results.

Ammonia and Nitrogen Dioxide Gas Sensing Properties

We demonstrate the application of the polymer sensing layers to the detection of NO_2 and NH_3 . The gaseous analytes in the experiments were prepared by controlled dilution with purified air and concentrations are reported in v/v form.

Figure 2 a-d displays the output characteristic of the FET-configured devices with an applied $V_{\text{g}} = -50$ V upon exposure to the various concentrations of NO_2 ranging from 0.5 ppm to 20 ppm with an exposure time of 3 minutes at each concentration. Note that the multiple plots on each graph correspond to different exposures; the gate voltage is kept constant. Figure 2 e-h displays the “transfer” characteristics of the devices corresponding to the measured output characteristics. Both transfer and output characteristics showed considerably increased currents for the PT-COOH while the PT-COOR, P3HT, and PQT12 had lesser responses but in the same direction. The on-current (I_{D}) increased continuously when the devices were exposed to consecutive increasing concentrations of NO_2 . It seems that at the measured 15 and 20 ppm of the PT-COOH, where we observe an overlay of the transfer and output characteristics, that at a measured I_{D} at -2.3×10^{-3} A, we may have reached the limitation of the semiconductor analyzer measuring capacity and therefore this may be a lower limit of the current. The dependence of the currents on V_{G} decreased for all the polymers except PQT12 with NO_2 exposure, indicating dominance of the conductance by NO_2 -induced charges. The dependence for PT-COOH even becomes anomalous at high exposures, indicating a possibly different response mechanism, as will be discussed below.

Figure 3 a-d displays the output characteristic of the FET at $V_{\text{g}} = -50$ V upon exposure to the various concentrations of NH_3 ranging from 0.5 ppm to 20 ppm with an exposure time of 3 minutes at each concentration. Figure 3 e-h displays the transfer characteristics of the FET pertaining to the measured output characteristics. P3HT and PQT12 both displayed typical p-type

behavior with exposure to NH_3 , where the NH_3 decreases the flow of the current in the channel and leads to a decrease in I_D . However, for both PT-COOH and PT-COOR, channel current surprisingly increases, and once again the dependence of I_D on V_G is decreased with the exposure.

In Figure S4 and Table S2 we have extracted and averaged the theoretical limits of detection (LOD) in the presence of NO_2 for PT-COOH, PT-COOR, P3HT, and PQT12 to be at 260 ± 90 ppb, 590 ± 70 ppb, 680 ± 110 ppb, and 1.1 ± 0.2 ppm, respectively by incorporating either a linear fit or power fit, or by converting a non-linear power to a linear function, where r^2 is the linear correlation coefficient (making sure $r^2 > 88\%$). (The short-term exposure limit for NO_2 is 1 ppm for 15 minutes, according to the National Institute for Occupational Safety and Health (NIOSH).) In order to extract LOD, either the common formula (concentration at which the signal is $(3 \cdot \text{standard deviation at lowest measured (0.5 ppm) concentration}) / (\text{slope of the line})$) is used if the function is linear^{41 a,b} or if the function is a power function^{41c} we extract the LOD as being expressed as the concentration where the measurement would equal the sample blank plus the standard deviation of analyte signal at the lowest measured concentration outlined in Table S2. The blank represents the environmental drift associated with the polymer sensing layer upon reaching stability. In these experiments, the drift of two successive scans was limited to no more than 1% current change. It has already been reported that at a film thickness of 585 nm, intentionally porous, spray-coated P3HT only responded to >10 ppm of NO_2 with response-concentration curves generally not intersecting the origin.⁴² P3HT blended with amine-donor polymers, on the other hand, reach a limit of detection of 240 ppb.⁴³ In addition, PQT12 has been reported to have a limit of detection to NO_2 as low as 32 ppb as a metal-semiconductor-metal (MSM) sensor, though the response-concentration plot used for the calculation had a y-intercept ("response" to zero analyte) higher than the response change at even 100 ppb.⁴⁴ Therefore, while the lower LOD associated with PT-COOH is significant, the limit of detection magnitudes are in the range of other thiophene polymer FETs and better than many. They could be decreased further using known methods such as more intense removal of possible electronically active impurities or adding porosity to the films.^{29, 45-51}

On the other hand, once the detection threshold is crossed, *the response per unit concentration change is unusually high*. For example, we obtain 1,030, 165, 20, and 12% response per ppm for PT-COOH, PT-COOR, P3HT, and PQT12, respectively, when exposed to NO_2 . We have extracted and compared this parameter from other published findings where pure P3HT in an OFET configuration showed about 10% response per ppm,⁴³ porous P3HT showed 20%/ppm,⁴² and for pristine PQT 12 in the MSM device, 200 sensitivity % response per ppm was obtained from a measurement under 100 ppb NO_2 , though almost the same % change in current was also obtained from exposures to higher concentrations.⁴⁴ It also further interesting to note that both PT-COOH and PT-COOR responses are fit to concentration raised the power of 2.7 and 1.5, while both P3HT and PQT12 display a linear response-concentration relation. This indicates that for both PQT12 and P3HT a first-order reaction where the response is proportional to the concentration of one NO_2 molecule is occurring, likely because of single molecule doping interactions. PT-COOR shows a somewhat super-linear response. However, PT-COOH displays a third-order response, suggesting a synergistic effect where NO_2 simultaneously increases hole transport and transport of protons on the carboxylic acid side chains.

In Figure S5 and Table S2, we have extracted theoretical LOD for PT-COOH, PT-COOR, P3HT, and PQT12 to be at 180 ± 80 ppb, 330 ± 120 ppb, 900 ± 400 ppb, and 850 ± 400 ppb of NH_3 , respectively. (The NIOSH short-term exposure limit is tens of ppm for hours of NH_3 exposure.) One study reported a distinct response to 100 ppb of NH_3 from commercial P3HT

deposited on a hydrophobic Si/SiO₂ substrate, but the additional response to 300 and 500 ppb was not significantly different.⁵² Another recent P3HT investigation only found responses to tens of ppm of NH₃.⁵³ It has been reported that P3HT and PQT12 have a limit of detection to NH₃ as low as 10 ppm using a TFT configuration⁵⁴ and 50 ppb as an organic vertical diode.⁵⁵ Again, our extracted theoretical limits of detection seem reasonable, and perhaps superior to other reports using thiophene polymer FETs. We obtain 110, 140, 13, and 27 sensitivity % response per ppm for PT-COOH, PT-COOR, P3HT, and PQT12, respectively, when exposed to NH₃. We have extracted and compared this parameter from other published findings where for P3HT in an OFET configuration, 10.6 sensitivity % response per ppm NH₃ in highly crystalline, aligned nanowires was found.⁵⁶ Pristine P3HT⁵⁴ and Pristine PQT 12⁴⁴ in OFETs were found to have <1 % response per ppm NH₃. The “vertical diode” geometry gave 60% per ppm response for both poly(alkylthiophenes).⁵⁵ Again looking at the best fit lines, P3HT and PQT12 both display a linear response indicating a one to one interaction with NH₃, while both PT-COOH and PT-COOR display a power order of 1.6 and 1.5 which may indicate the influence that a carboxylic acid and ester have with NH₃ due to the ordering effects that result.

The sensitivities of all four polymer sensing layers, based on FET responses to the cumulative exposures and extracted from -50 V bias voltage data, are shown in Figure 4. Figure 4A displays the response to continuous exposure to NO₂ while Figure 4B displays the response to continuous exposure to NH₃. The sensitivity is calculated as the relative change in sensor current due to the prescribed cumulative gas exposure (all exposures up to each x-axis value) which is defined as:

$$S (\%) = \frac{I_{Gas} - I_{Air}}{I_{Air}} \times 100\% ;$$

where I_{Air} is the initial current measured in ambient air, and I_{Gas} is the current under either NO₂ or NH₃ gas exposure.

We also repeated the same set of measurements of response to NO₂ for PT-COOH, PT-COOR, P3HT, and PQT12, as shown in Figure S6, with a continuous real-time transient response curve displaying the polymer response to 180 seconds of exposure duration to NO₂, followed by 12 minutes recovery, and repeating with subsequent higher exposure from 0.5 ppm to 20 ppm. Afterwards, a recovery period was evaluated after 20 ppm exposure and displayed in Figure S7. Overall, PT-COOH has a striking response and recovery characteristic. Looking at Figure S6 a-d, it is observed that at smaller concentrations from 0.5-5 ppm, PT-COOH has a more delayed response to NO₂ where as soon as the gas is turned off the polymer will continue to show an increase in current for an additional 450 seconds before reaching a period of stability. This may further support that the mechanistic interaction of the carboxylic acid moiety, which may include a slow reorganization of NO₂ and protons, greatly differing from that of P3HT. After 5 ppm exposure, PT-COOH shows a decrease in current upon immediate change of gas to purified air. P3HT, on the other hand, immediately begins to recover once NO₂ is displaced and the PT-COOR displays intermediate behavior to both P3HT and PT-COOH. Furthermore, looking at Figure S7 a-d, we further analyze the full recovery after 20 ppm exposure of NO₂. We fit an exponential decay line that follows $y = A * e^{kx}$ where x is decay time in seconds. Within 1 hour at ambient temperature, PT-COOH displays 93% recovery, while PT-COOR and P3HT display comparable recovery at 75% and 67%, respectively. PQT12 displayed more sluggish response and recovery of 37%. Although an hour to achieve nearly complete recovery is neither outstanding nor competitive for use where rapid reversibility is crucial, it is interesting to note

that the carboxylic acid functional group decreases the recovery time significantly. Additional energetic input such as thermal activation or even placing under vacuum will result in the acceleration of NO_2 desorption and regeneration process.⁵⁷ To compare this to already published response evolutions, there have been prior reports for transient response to NO_2 exposure for P3HT (but not for PQT12) that would allow fair comparisons, though this literature is inconsistent. One reference reports that P3HT has a 400% response to an exposure of 20 ppm and has a recovery of roughly 30 minutes⁴² while another reports 10% response at 20 ppm exposure with 5 minute recovery.⁵⁸ It is interesting to report that both groups airbrushed the polymer in order to maximize surface area and create porosity which might be another option that may affect recovery response acceleration.

Additionally, the repetition of the real time transient response and recovery curve with PT-COOH and PT-COOR with exposure to NH_3 was performed, with results displayed in Figure S8 a-b. The recovery period was further evaluated in Figure S8 c-d. PT-COOH and PT-COOR both display similar trends and response to NH_3 . Again, the above-mentioned increase in current is observed for both polymers up toward 5-10 ppm of NH_3 exposure. However, afterwards the magnitude of response begins to decrease. It is probable that there may possibly be 2 mechanistic interactions taking place. At low concentrations of NH_3 , the proton of NH_3 will be incorporated into a hydrogen bond network with the binding moieties of the carboxylic acid and ester. This will result in intermolecular conduction being enhanced. Afterwards, once the network is completely filled, the next available interaction is the normal expected donation of the ammonia lone pairs to quench the holes, which results in the decrease in the magnitude of response because we now have switched the primary mechanistic interaction to the secondary interaction. Additionally, it is observed that PT-COOH recovers more slowly than PT-COOR. Within 1 hour, PT-COOH recovers only 40% while PT-COOR recovers at 70% in ambient room temperature condition. This is possibly due to hydrogen bonding interactions being stronger in PT-COOH than PT-COOR where an ester cannot form intermolecular hydrogen bonding with other esters while carboxylic acids have this capability. Unfortunately, we were unable to perform the analogous characterization for P3HT and PQT12 because the response was too low compared to the drift. However, looking at reported literature, pristine PQT12 was found to have a 12% response at 20 ppm exposure of NH_3 with a full recovery time of about 8 minutes,⁵⁹ while P3HT blended with polystyrene showed a 40% response with exposure to 20 ppm of NH_3 and a recovery of roughly 20 minutes.⁴⁶ Polymers with functional groups that can hydrogen bond with NH_3 appear to respond and recover more slowly while polymers with plain alkyl chains recover faster.

The PT-COOH has a remarkable cumulative response to NO_2 of roughly 15,000% increase in I_D , before reaching a plateau around 10 ppm exposure. Looking at the inset in Figure 4A, PT-COOR has a significant increase in current as well starting with an initial exposure to 0.5 ppm but continues to increase even with exposure to 20 ppm of NO_2 ; however, it reaches a maximum of only 1200%. P3HT response reaches 300% and PQT12 shows the lowest at a response maximum of 70%. Regarding NH_3 exposure (Figure 4B), PQT12 and P3HT display, as expected, a decrease in channel current where I_D decreases 50% and 30%, respectively in response to 1-2 ppm NH_3 . However, PT-COOH and PT-COOR display an *increase* in current with exposure to NH_3 reaching a maximum cumulative response of 300% and 450%, respectively, when exposed to 20 ppm of NH_3 . As mentioned above, this behavior deviates from typical p-type polymer responses. To compare these results with already published findings, PQT12 was reported by our group to show an increase in I_D of 14% with 1 ppm NO_2 exposure

and 200% at 5 ppm NO₂ exposure at 5 minutes of exposure duration.⁶⁰ P3HT has been reported to show a current increase of 100% at 5 ppm NO₂ exposure.⁶¹ These values do not significantly deviate from our experimental findings where at 1 ppm NO₂ exposure for PQT12 and P3HT we obtained a comparable cumulative increase in I_D of 17% for both polymers. In comparison with our NH₃ study, prior publications from our group and others have reported a similar decrease in I_D at 30%-50% with 1 ppm of NH₃ exposure for P3HT and PQT12.^{47,56} Our present results show a decrease in I_D at 18% and 28% with 1 ppm of cumulative NH₃ exposure for P3HT and PQT12 for 3 minutes. Considering differences in sample morphology and exposure methods, our NH₃ results on non-carboxylated polythiophenes are consistent with prior reports.

RG Platform to Elucidate Gas Mechanism

In a recent publication, we had developed a way to characterize dopant effects and diffusion in polymers using a remote-gate field transistor (RG FET) setup which allowed us to measure changes to the surface potential of the polymer film on the RG which is coupled to the oxide gate of the commercial silicon FET (Scheme S2).⁶² We extend this application and employ it to elucidate the mechanism of interaction that is occurring with the polymers being exposed to the NO₂ and NH₃.

The polymer sensing layer was spin-coated onto a Si/SiO₂ (300 nm thermal oxide) substrate to form the RG and was coupled to the gate of the commercial silicon FET transistor. The silicon FET equilibrated to the interfacial potential of the polymer sensing layer with a drop of acetonitrile that also served as the contact solvent between the surface of the polymer and two Ag/AgCl reference electrodes. Acetonitrile is our chosen contact choice because it is a polar aprotic solvent with small but sufficient conductivity for this purpose, chemically stable, and a non-solvent of our chosen polymers. If there is any change in the surface potential of the polymer RG, the FET will report this change by means of the V_{TH, RG} shift. Depending on the direction and magnitude of this shift, we can gain information about the mechanism of interaction between the sensing layers and analyte vapors.

Figure 5 a-d displays the transfer curves of the RG FET coupled with each of our polymer sensing layers. Initially we obtain potential of our FET to the equilibrated interfacial potential of our polymer RG with just ACN, which marks our equilibrated baseline. When we remove our polymer RG and expose it without the ACN for 20 minutes to either 1 ppm or 20 ppm of NO₂, recouple the RG to the RG FET platform, and then remeasure the remote-gate field effect transistor, we see a horizontal shift to the left which indicates an additional positive interfacial potential between the ACN and the polymer, which could arise from induced holes in the sensing layer and counterions closer to the ACN. We also analyze the recovery in order to determine whether this interaction is reversible or whether it results in a more permanent chemical change to the polymers. We found that each polymer is restored completely to its initial electronic state when baking at 60°C and under vacuum for 1 hr after gas exposure, which implies that NO₂ is reversibly adsorbing to the surface of the polymer sensing layer.

Figure 5 e-h further analyzes the change to the V_{TH, RG}. Twenty consecutive scans are applied in order to determine stability or possible drift of the response. When stabilizing the polymer RG to the FET with ACN we obtain either no drift or a modest drift that stabilizes after 10-20 scans. However, once we remeasure with the exposure to either 1 ppm NO₂ or 20 ppm NO₂ there is an observable decrease in the V_{TH, RG}, with the shift magnitude higher for the higher exposure concentration amount. The shift is only slowly reversible, even in the presence of ACN, except

for PQT12. The most stable response is from PT-COOH. This could indicate a stronger, though still reversible, physical adsorption interaction that the carboxylic acid terminal side chain has with NO₂ compared to the other 3 polymer sensing layers. The response magnitudes are illustrated as a bar graph in Figure S9.

We repeated these experiments with exposure of the polymer RGs to NH₃. This time, there was negligible shift in the V_{TH} towards accumulation for the carboxyl polymers and no discernable change for the alkyl polymers (Figure 5 e-h). This implies that a different type of interaction occurs on the polymer sensing layer. A small amount of hole quenching or COOH ionization could be responsible for the small shift that we observe for the carboxyl polymers. However, it seems that NH₃ is much more readily desorbed from the polymers by ACN than is NO₂, since the alkyl polymer FETs showed significant conductance decreases from NH₃ as expected. Also, this experiment indicates that the conductance increase observed as the FET response by the carboxyl polymers is not from p-doping, which would not be expected from NH₃ anyway. N-doping by NH₃ would be consistent with the RG response and with the possible ambipolarity of the carboxyl polymers, though this is also not predictable from the polymer chemical structures. One other possibility is the proton conduction through H-bond rearrangements leads to ionic current that adds to the current observed before exposures of carboxyl polymer FETs.

In Figure S10, we show data from transconductance (G_m) measurements. G_m is maintained at constant values of 67 μS, 65.5 μS, 65 μS, and 64 μS for PT-COOH, PT-COOR, P3HT, and PQT12, respectively. These results imply that there is no gate voltage-dependent change in the interfacial potential or series impedance caused by any of the coatings or exposures.

Figure S11 (a,c), shows the result of repeated exposure of the bare Si/SiO₂ substrate to NO₂ and NH₃; however, little to no shift was observed which indicates that the defined gases are not interacting with, inducing charge carriers in, or causing a chemical reaction with the oxide. This is further reflected in the transconductance of the Si/SiO₂ substrate not changing either (Figure S11 b,d).

Evaluating these results, we can infer that the increase in conductance of polymer FETs with NO₂ gas is due to the charge transfer taking place between the film and NO₂. The similarity of the ionization potential of thiophene polymers and the reduction potential of NO₂ in condensed phases makes some degree of doping, and associated hole generation, thermodynamically probable. The particularly strong response by the COOH polymer could be due to its greater binding capability and/or retention of NO₂ compared to the other thiophene polymers.

In order to extract hole concentration and mobility changes induced by NO₂ exposure (unfortunately, we could not apply this analysis to the hole quenching by NH₃ exposure due to the insignificant ΔV_{Th, RG} shift when exposed to that gas) we use two equations as we have done in prior work:⁶²

$$\sigma = e \cdot \mu_h \cdot p ;$$

where σ is defined as the experimental conductivity, μ_h is the hole mobility, and p is the carrier concentration. Table S3, compiles the parameters measured on the unexposed polymer sensing RGs as well as the gas-exposed RGs. In order to obtain the hole mobility when exposed to NO₂, we used the second equation⁶²:

$$p_d = p_0 \cdot \exp \left(- \frac{\Delta V_{Th, RG}}{KBT} \right) ;$$

The $\Delta V_{Th, RG}$ was extracted from the FET transfer curve shift. It is gratifying to observe that the calculated mobilities (except for PT-COOH) are slightly higher than the FET mobilities, consistent with NO₂ exposure filling lower energy/lower mobility states, and otherwise validating the charge densities calculated from σ and p_d , again except for PT-COOH, which has a likely contribution from proton conduction as discussed below.

In Figure 6 the hole concentration (A), and mobility (B), and conductivity (C) are plotted for each polymer sensing layer and NO₂ exposure (again recalling that for the carboxylated polymers, mobility from the unexposed FET is only a rough estimate). It is observed that the apparent hole concentration increases dramatically for PT-COOH, and substantially for PT-COOR, P3HT, and PQT12. In order to evaluate the plausibility of the calculated charge densities, we estimated a theoretical charge carrier density saturation magnitude. Let us assume that there should be approximately 10 monomer units between 2 positive charges. We obtain this assumption based on published optical absorption spectra determining the spatial extent of one positive polaron to be delocalized over 8.6 repeat units on poly(3-decylthiophene) (P3DT)⁶³. However, order, crystallinity, and hydrogen interaction between adjacent repeat units are contributing factors to the delocalization distance.⁶⁴⁻⁷⁰ Molecular volume is calculated in cubic centimeters per mole (cm³ per Avogadro's number N of molecules, equal to molecular weight, which in turn is grams per N , assuming a density of 1); therefore:

$$\text{Saturated Charge Carrier Density } (p_{\text{sat}}) = \frac{N}{\text{Molecular Volume}};$$

where molecular volume denotes the volume that a ten-ring length of each polythiophene would encompass. Therefore, we expect a total charge concentration to be allowed on a polythiophene unit to be $7 \times 10^{20} \text{ cm}^{-3}$.⁷¹⁻⁷² When looking at Figure 6A, we can see that the apparent charge density for PT-COOH exceeds this estimate for the allowed hole concentration. PT-COOR, P3HT, and PQT12, on the other hand, show charge densities that fall well below this theoretical saturation, and are thus plausible quantities. Therefore, we propose that the carboxylic acid functional group acts as a source of conductive protons that add positive current to the hole current flowing through the polymer main chains. Therefore, the substantial sensitivity of PT-COOH to NO₂ in comparison to PT-COOR, P3HT, and PQT12 can include an increase in the proton as well as hole current.

With respect to the mechanism of the NH₃ response, it is generally accepted that NH₃ reduces the current flowing in the p-type conducting channel because of lone pairs neutralizing holes.^{29, 46, 48} In our study, PQT12 and P3HT display this behavior, as has been shown before. However, PT-COOH and PT-COOR have a completely inverse effect where the current is actually increasing. We hypothesize that this may be occurring due to the hydrogen bonding moieties of the carboxylic acid and ester being able to physisorb NH₃ which may cause a change in the distribution of charge, rearrange polymer chains, and/or create a proton transfer network that causes the increase of flowing current in the device channel. A recent study reported the hydrogen bonding-directed assembly of carboxylic acid-functionalized poly(3-alkylthiophene) derivatives.⁷³ Changes in hydrogen bonding around a thiophene carboxylic acid polymer caused by a solvent with different hydrogen bonding properties induced morphological changes that could affect charge transport. There is another possibility that the compensation of oxidant from the ambient environment by the reducing effect of NH₃ is as large in PT-COOH as it may be in other hole-carrying polymers in which NH₃ may deplete holes that are originally present.⁵²

◆ Conclusion

In summary, we report a polymer-based chemiresistive sensing device for NO₂ and NH₃ detection with remarkably high response per increment of exposure by exploiting thiophene conjugated polymers with carboxylic acid and ester terminal side chains. NO₂ sensitivity was dramatically higher and more superlinear for the carboxylic acid compared to the ester counterpart. The acid and ester showed high and comparable sensitivity to NH₃. All these responses resulted in conductance increasing, which for the case of NH₃ was unexpected, especially for a p-type polymer. Non-carboxylated polymers showed the expected conductance increases and decreases for NO₂ and NH₃, respectively. We also utilize a new technique, the remote gate (RG) detection platform, in order to understand the mechanism associated behind the polymer sensing layers' responses to the gas exposures. We thus confirmed that two differing mechanisms are occurring. Overall, we believe the high sensitivity and unexpected NH₃ response sign of the carboxylic acid and ester polymers were attributed to multiple possible interactions involving protons in the system. The unusual NO₂ response ratios and the counterintuitive carboxylated thiophene responses to NH₃ could provide additional elements of selectivity to response patterns of polymer semiconductor arrays to gaseous analytes.

◆ Associated Content

Supporting Information

Synthetic procedures, tabulated characterization data, copies of spectra, and electronic characterization of the materials presented in this work.

◆ Author Information

Corresponding Author

*E-mail: hekatz@jhu.edu

Notes

The authors declare no competing financial interest.

Acknowledgements

We thank the National Science Foundation, grant numbers ECCS 1807293 (organic transistor and vapor exposure studies) and DMR 1807292 (RG investigations) for funding. The authors also would like to thank Professor Rebekka Klausen (Johns Hopkins University) and Yuyang Ji for use of the GPC facility.

References

1. Yamazoe, N.; Miura, N. Environmental gas sensing. *Sensors Actuators B Chem.* **1994**, *20*: 95-102.
2. Hong, H.S.; Phuong, N.H.; Huong, N.T.; Nguyen, H.N.; Nguyen, T.H. Highly sensitive and low detection limit of resistive NO₂ gas sensor based on a MoS₂/graphene two-dimensional heterostructures. *Applied Surface Science.* **2019**, *492*: 449-454.
3. Duk-Dong, L.; Dae-Sik, L. Environmental gas sensors. *IEEE Sensors J.* **2001**, *1*: 214-224.
4. Wetchakun, K.; Samerjai, T.; Tamaekong, N.; Liewhiran, C.; Siriwong, C.; Kruefu, V.; Wisitsoraat, A.; Tuantranont, A.; Phanichphant, S. Semiconducting metal oxides as sensors for environmentally hazardous gases. *Sensors Actuators B Chem.* **2011**, *160* (1): 580-591.
5. Fine, G.F.; Cavanagh, L.M.; Afonja, A.; Binions, R. Metal Oxide Semiconductor gas sensors in environmental monitoring. *Sensors.* **2013**, *10*: 5469-5502.
6. Wallin, M.; Karlsson, C.-J.; Skoglundh, M.; Palmqvist, A. Selective catalytic reduction of NO_x with NH₃ over zeolite H-ZSM-5: influence of transient ammonia supply, *J. Catal.* **2003**, *218*: 354-364.
7. Xuan, X.; Yue, C.; Li, S.; Yao, Q. Selective catalytic reduction of NO by ammonia with fly ash catalyst, *Fuel* **82**, 2003: 575-579.
8. Satake, K.; A. Kobayashi, A.; Nakahara, T.; Taekeuchi, T. NO_x sensor for exhaust monitoring, *Digest* 98
9. Mount, G.H.; Rumburg, B.; Havig, J.; Lamb, B.; Westberg, H.; Yonge, D.; Johnson, K. Kincaid, K. Measurement of atmospheric ammonia at a dairy using differential optical absorption spectroscopy in the mid-ultraviolet, *Atmos. Environ.* **2002**, *36*: 1799-1810.
10. Durbin, T.D.; Wilson, R.D.; Norbeck, J.M.; Miller, J.W.; Huai, T.; Rhee, S.H. Estimates of the emission rates of ammonia from light-duty vehicles using standard chassis dynamometer test cycles, *Atmos. Environ.* **2002**, *36*: 475-1482.
11. Moos, R.; Muller, R.; Plog, C.; Knezevic, A.; Leye, H.; Irion, E.; Braun, T.; Marquardt, K.-J.; Binder, K. Selective ammonia exhaust gas sensor for automotive applications, *Sens. Actuators B.* **2002**, *83*:181-189.
12. S. Budarvari, et al., *The Merck Index, An Encyclopedia of Chemicals, Drugs and Biologicals*, 12th ed., Merck, 1996.
13. Close, L.G.; Catlin, F.I.; Cohn, A.M. Acute and chronic effects of ammonia burns on the respiratory tract, *Arch. Otolaryngol.* **1980**, *106* (3): 151-158.
14. Leung, C.M.; Foo, C.L. Mass ammonia inhalation burns—experience in the management of 12 patients, *Ann. Acad. Med. Singapore* **21**, **1992**, *21* (5): 624-629.
15. de la Hoz, R.E.; Schueter, D.P.; Rom. W.N. Chronic lung disease secondary to ammonia inhalation injury: a report on three cases, *Am. J. Ind. Med.* **1996**, *29* (2): 209-214.
16. Michaels, R.A. Emergency planning and acute toxic potency of inhaled ammonia, *Environ. Health Perspect.* **1999**, *107* (8): 617-627
17. Ament, W.; Huizenga, J.R.; Kort, E.; van der Mark, T.W.; Grevink, R.G.; Verkerke, G.J. Respiratory ammonia output and blood ammonia concentration during incremental exercise, *Int. J. Sports Med.* **1999**, *20* (2): 71-77.
18. Khan, M.A.H.; Rao, Mulpuri, Li, Q. Recent advances in electrochemical sensors for detecting toxic gases: NO₂, SO₂ and H₂S. *Sensors*, **2019**, *19*: 905.

19. Zhang, Y. X.; Kim, J. J.; Chen, D.; Tuller, H. L.; Rutledge, G. C. Electrospun Polyaniline Fibers as Highly Sensitive Room Temperature Chemiresistive Sensors for Ammonia and Nitrogen Dioxide Gases. *Adv. Funct. Mater.* **2014**, 24, 4005–4014.
20. Maynor, M. S.; Nelson, T. L.; O'Sullivan, C.; Lavigne, J. J. A Food Freshness Sensor Using the Multistate Response from Analyte- Induced Aggregation of a Cross-Reactive Poly(thiophene). *Org. Lett.* **2007**, 9, 3217–3220.
21. Shustova, N. B.; Cozzolino, A. F.; Reineke, S.; Baldo, M.; Dinca, M. Selective Turn-On Ammonia Sensing Enabled by High-Temperature Fluorescence in Metal–Organic Frameworks with Open Metal Sites. *J. Am. Chem. Soc.* **2013**, 135, 13326–13329.
22. Markovics, A.; Kovacs, B. Fabrication of Optical Chemical Ammonia Sensors Using Anodized Alumina Supports and Sol–Gel Method. *Talanta* **2013**, 109, 101–106.
23. Nelson, T. L.; Tran, I.; Ingallinera, T. G.; Maynor, M. S.; Lavigne, J. J. Multi-Layered Analyses Using Directed Partitioning to Identify and Discriminate between Biogenic Amines. *Analyst* **2007**, 132, 1024– 1030.
24. Karpas, Z.; Tilman, B.; Gdalevsky, R.; Lorber, A. Determination of Volatile Biogenic Amines in Muscle Food Products by Ion Mobility Spectrometry. *Anal. Chim. Acta* **2002**, 463, 155–163.
25. Liu, S. F.; Petty, A. R.; Sazama, G. T.; Swager, T. M. Single- Walled Carbon Nanotube/Metalloporphyrin Composites for the Chemiresistive Detection of Amines and Meat Spoilage. *Angew. Chem., Int. Ed.* **2015**, 54, 6554–6557.
26. Zhou, J.; Lin, H. Chen, X.F.; Shu, J.; He, J.H.; Li, H.; Xu, Q.F.; Li, N.J.; Chen, D.Y.; Lu, J.M. Ultrasensitive and robust organic gas sensors through dual hydrogen bonding. *Materials Horizons.* **2019**, 6 (3): 554-562.
27. Song, Y.G.; Shim, Y.S.; Suh, J.M.; Kim, G.S.; Choi, K.S.; Jeong, B.; Kim, S.; Jang, H.W.; Ju, B.K.; Kang, C.Y. Ionic-Activated chemiresistive gas sensors for room temperature operation. *Small.* **2019**, 15 (40): 1902065
28. Yu, C.; Lin, H.Z.; Zhou, J.; Cheng, X.F.; He, J.H.; Li, H.; Xu, Q.F.; Li, N.J.; Chen, D.Y.; Lu, J.M. An ion-in-conjugation polymer enables the detection of NO₂ with parts-per-trillion sensitivity and ultrahigh selectivity. *J. Mater. Chem. A.* **2020**, Advance Article.
29. Lv A, Pan Y, Chi L. Gas sensors based on polymer field-effect transistors. *Sensors.* **2017**, 17(1): 213.
30. D. M. Wilson, S. Hoyt, J. Janata, K. Booksh, L. Obando, *IEEE Sens. J.* **2001**, 1, 256.
31. Fichou a, D.; Horowitz b, G. Molecular and Polymer Semiconductors, Conductors, and Superconductors: Overview. *Encyclopedia of Materials: Science and Technology 2nd Edition*, **2001**, 5748-5757
32. Yang, Y.; Zhang, G.; Luo, H.; Liu, Z.; Zhang, D. Highly sensitive thin-film field-effect transistor sensor for ammonia with the DPP-Bithiophene conjugated polymer entailing thermally cleavable tert-butoxy groups in the side chains. *ACS Appl. Mater. Interfaces* **2016**, 8: 3635-3643.
33. Dong, K.Y.; Choi, J.; Lee, Y.D.; Kang, B.H.; Yu, Y.Y.; Choi, H.H.; Ju, B.K. Detection of a CO and NH₃ gas mixture using carboxylic acid-functionalized single-walled carbon nanotubes. *Nanoscale Res Lett.* **2013**, 8 (1): 12
34. Hintz, H.; Peisert, H.; Egelhaaf, H.J.; Chasse, T. Reversible and irreversible light-induced p-doping of P3HT by oxygen studied by photoelectron spectroscopy (XPS/UPS). *J. Phys. Chem. C*, **2011**, 115: 13373-13376.

35. Schweiger, T.; Liu, X.; Peisert, H.; Adolphi, B.; Kiriya, N.; Knupfer, M. Electronic properties of interfaces between different sexithiophenes and gold. *J. Appl. Phys.*, **2005**, *97*: 123712.
36. Kerber, S.J.; Bruckner, J.J.; Wozniak, K.; Seal, S.; Hardcastle, S.; and Barr, T.L. The nature of hydrogen in x-ray photoelectron spectroscopy: general patterns from hydroxides to hydrogen bonding. *Journal of Vacuum Science & Technology A: Vacuum, Surfaces, and Films*. **1996**, *14* (3): 1314-1320.
37. Stevens, J.S.; Byard, S.J.; Seaton, C.C.; Sadiq, G.; Davey, R.J.; Schroeder, S.L.M. Proton transfer and hydrogen bonding in the organic solid state: a combined XRD/XPS/ssNMR study of 17 organic acid-base complexes. *Phys. Chem. Chem. Phys.* **2014**, *16*, 1150-1160.
38. Lopez, G.P.; Castner, D.G.; Ratner, B.D. XPS O 1s binding energies for polymers containing hydroxyl, ether, ketone, and ester groups. *Surface and Interface Analysis*. **1991**, *17*(5): 267-272.
39. Freudenberg, U.; Zschoche, S. Simon, F.; Janke, A.; Schmidt, K.; Behrens, S.H.; Auweter, H.; Werner, C. Covalent immobilization of cellulose layers onto malice anhydride copolymer thin films. *Biomacromolecules*. **2005**, *6*(3): 1628-1634.
40. Martínez Hardigree, J.F.; Katz, H.E. Through thick and thin: tuning the threshold voltage in organic field-effect transistors. *Acc. Chem. Res.*, **2014**, *47*: 1369-1377.
41. a) Belter, M.; Sajnóg, A.; Barańkiewicz, D. Over a century of detection and quantification capabilities in analytical chemistry-historical overview and trends. *Talanta*, **2014**, *129*: 606-616. b) Linnet, K.; Kondratovich, M. Partly nonparametric approach for determine the limit of detection. *Clin Chem*, **2004**, *50* (4): 732-740. c) Shrivastava, A.; Gupta, V.B. Methods for the determination of limit of detection and limit of quantitation of the analytical methods. *Chronicles of Young Scientists*, **2011**, 21-25
42. Yang, J.; Xie, G.Z.; Su, Y.J.; Zhang, Q.P.; Du, H.F.; Tai, H.L.; Du, X.S.; J. Y.D. Flexible organic thin-film transistors based on poly(3-hexylthiophene) films for nitrogen dioxide detection. *Science China Technological Sciences*, **2018**, *61* (11): 1696-1704.
43. Han, S.; Yang, Z.; Li, Z.; Zhuang, X.; Akinwande, D.; Yu, J. Improved room temperature NO₂ sensing performance of organic field-effect transistor by directly blending a hole-transporting/electron-blocking polymer into the active layer. *ACS App. Mater. Interfaces*, **2018**, *10*: 38280-38286.
44. Kumar, C.; Rawat, G.; Kumar, H.; Kumar, Y.; Ratan, S.; Prakash, R.; Jit, S. Poly(3,3''-didodecyl quarter thiophene) based flexible nitrogen dioxide gas sensor. *IEEE Sensors Letters*, **2018**, *2* (1): Art no. 4500104.
45. Lee, Y.H.; Jang, M.; Lee, M.Y.; Kweon, O.Y.; Oh, J.H. Flexible field-effect transistor-type sensors based on conjugated molecules. *Chem*, **2017**, *3*: 724-763.
46. Han, S.J.; Zhuang, X.M.; Shi, W.; Yang, X.; Li, L.; Yu, J.S. Poly(3-hexylthiophene)/polystyrene (P3HT/PS) blends based organic field-effect transistor ammonia gas sensor. *Sens. Actuator B Chem*. **2016**, *225*:10-15
47. Besar, K.; Yang, S.; Guo, X.G.; Huang, W.; Rule, A.M.; Breyse, P.N.; Kymissis, I.J.; Katz H.E. Printable ammonia sensor based on organic field effect transistor. *Org. Electron.*, **2014**, *15*:3221-3230.
48. Zan, H.W.; Li, C.H.; Yu, C.K.; Meng, H.F. Sensitive gas sensor embedded in a vertical polymer space-charge-limited transistor. *Appl. Phys. Lett.* **2012**, *101*:023303

49. Klug, A.; Denk, M.; Bauer, T.; Sandholzer, M.; Scherf, U.; Slugovc, C.; List, E.J.W. Organic field-effect transistor-based sensors with sensitive gate dielectrics used for low-concentration ammonia detection. *Organic Electronics*, **2013**, 14 (2): 500-504.
50. Mirza, M.; Wang, J.; Wang, L.; He, J.; Jiang, C. Response enhancement mechanism of NO₂ gas sensing in ultra-thin pentacene field-effect transistors. *Organic Electronics*, **2015**, 24: 96-100.
51. Bannock, J.H.; Treat, N.D.; Chabynyc, M.; Stingelin, N.; Heeney, M.; de Mello, J.C. The influence of polymer purification on the efficiency of poly(3-hexylthiophene): fullerene organic solar cells. *Sci Rep.*, **2016**, 6: 23651.
52. Tiwari, S.; Singh, A.K.; Joshi, L.; Chakrabarti, P.; Takashima, W.; Kaneto, K.; Prakash, R. Poly-3-hexylthiophene based organic field-effect transistor: detection of low concentration of ammonia. *Sensors and Actuators B: Chemical*, **2012**, 171: 962-968.
53. Cavallari, M.R.; Izquierdo, J.E.E.; Braga, G.S.; Dirani, E.A.T.; Pereira-da-Silva, M.A.; Rodríguez, E.F.G.; Fonseca, F.J. Enhanced Sensitivity of Gas Sensor Based on Poly(3-hexylthiophene) thin-film transistors for disease diagnosis and environment monitoring. *Sensors*, **2015**, 15: 9592-9609.
54. Jeong, J.W.; Lee, Y.D.; Kim, Y.M.; Park, Y.W.; Choi, J.H.; Park, T.H.; Soo, C.D.; Won, S.M.; Han, I.K.; Ju, B.K. The response characteristics of a gas sensor based on poly-3-hexylthiophene thin-film transistors. *Sens. Actuators B Chem.* **2010**, 146: 40-45.
55. Dai, M.Z.; Chen, Y.H.; Chuang, M.Y.; Zan, H.W.; Meng, H.F. Achieving a good lifetime in a vertical organic diode gas sensor. *Sensors*, **2014**, 14: 16287-16295.
56. Mun, S.; Park, Y.; Yong-Eun, K.L.; Sung, M.M. Highly sensitive ammonia gas sensor based on single-crystal poly(3-hexylthiophene) (P3HT) organic field effect transistor. *Langmuir*, **2017**, 33 (47): 13554-13560.
57. Procek, M.; Kepska, K.; Stolarczyk, A. A study on the impact of Poly(3-hexylthiophene) chain length and other applied side-chains on the NO₂ sensing properties of conducting graft copolymers. *Sensors*, **2018**, 18 (3): 928.
58. Xie, T.; Xie, G.Z.; Zhou, Y.; Huang, J.; Wu, M.; Jiang, Y.; Tai, H. Thin film transistors gas sensors based on reduced graphene oxide poly(3-hexylthiophene) bilayer film for nitrogen dioxide detection, *Chemical Physics Letters*, **2014**, 614: 275-281.
59. Kumar, C.; Rawat, G.; Kumar, H.; Kumar, Y.; Prakash, R.; Jit, S. Electrical and ammonia gas sensing properties of PQT-12/CdSe quantum dots composite-based organic thin film transistors. *IEEE Sensors Journal*, **2018**, 18, 6085-6091.
60. Li, H.; Dailey, J.; Kale, T.; Besar, K.; Koehler, K.; Katz, H.E. Sensitive and selective NO₂ sensing based on alkyl- and alkylthio-thiophene polymer conductance and conductance ratio changes from differential chemical doping. *ACS Appl. Mater. Interfaces*, **2017**, 9 (24), 20501-20507.
61. Xie, T.; Xie, G.; Du, H.; Zhou, Y.; Xie, F.; Jiang, Y.; Tai, H. The fabrication and optimization of thin-film transistors based on poly(3-hexylthiophene) films for nitrogen dioxide detection. *IEEE Sensors Journal*, **2016**, 16 (7): 1865-1871.
62. Jang, H.J.; Wagner, J.; Li, H.; Zhang, Q.; Mukhopadhyaya, T.; Katz, H.E. Analytical platform to characterize dopant solution concentrations, charge carrier densities in films and interfaces, and physical diffusion in polymers utilizing remote field-effect transistors. *J. Am. Chem. Soc.* **2019**, 141 (12): 4861-4869.

63. Takeda, N.; Miller, J.R. Poly(3-decylthiophene) radical anions and cations in solution: single and multiple polarons and their delocalization lengths in conjugated polymers. *J. Phys. Chem. B*, **2012**, 116: 14715-14723.
64. Steyrleuthner, R.; Zhang, Y.; Zhang, L.; Kraffert, F.; Cherniawski, B.P.; Bittl, R.; Briseno, A.L.; Bredas, J.; Behrends, J. Impact of morphology on polaron delocalization in a semicrystalline conjugated polymer. *Phys. Chem. Chem. Phys.*, **2017**, 19: 3627
65. Zhang, Y.; Steyrleuthner, R.; Bredas, J. Charge delocalization in oligomers of poly(2,5-bis(3-alkylthiophene-2-yl)thienol[3,2-b]thiophene)(PBTTT). *J. Phys. Chem. C.*, **2016**, 120: 9671-9677.
66. Bakalis, J.; Cook, A.R.; Asaoka, S.; Forster, M.; Scherf, U.; Miller, J.R. Polarons, compressed polarons, and bipolarons in conjugated polymers. *J. Phys. Chem. C*, **2014**, 118: 114-125.
67. Rao, B. K.; Kestner, N. R.; Darsey, J. A. Interring Rotational Potential of Biphenyl and Its Effect on Poly(Para-Phenylene). *Z. Phys. D: At., Mol. Clusters* **1987**, 6, 17-20.
68. Momicchi, F.; Bruni, M. C.; Baraldi, I. Fluorescence and Absorption-Spectra of Polyphenyls - Theoretical Study on Band Shape. *J. Phys. Chem.* **1972**, 76, 3983-3990.
69. Tretiak, S.; Saxena, A.; Martin, R. L.; Bishop, A. R. Conformational Dynamics of Photoexcited Conjugated Molecules. *Phys. Rev. Lett.* **2002**, 89, 097402.
70. Takeda, N.; Asaoka, S.; Miller, J. R. Nature and Energies of Electrons and Holes in a Conjugated Polymer, Polyfluorene. *J. Am. Chem. Soc.* **2006**, 128, 16073-16082.
71. S. Schlick, *Advanced ESR Methods in Polymer Research*, John Wiley & Sons, Inc., 2006.
72. Zhang, X.; Li, Z.; Lu, G. First-principles determination of charge carrier mobility in disordered semiconducting polymers. *Physical Review B*. **2010**, 82: 205210.
73. Bilger, D.W.; Figueroa, J.A.; Redeker, N.D.; Sarkar, A.; Stefik, M.; Zhang, S. Hydrogen-bonding-directed ordered assembly of carboxylated poly(3-Alkylthiophene)s. *ACS Omega*, **2017**, 2 (11): 8526-8535.

Figure Captions:

Scheme 1. Schematic architecture of the gas sensing device is based on a bottom-gate, top-contact OFET structure with a semiconducting polymer serving as the organic active layer. A heavily doped p-type Si wafer and a layer of dry oxidized SiO₂ (300 nm) were used as a gate electrode and gate dielectric layer, respectively. R denotes either PT-COOH, PT-COOR, P3HT, and PQT12 with exposure to either NO₂ or NH₃.

Figure 1. Transfer characteristic for polymer sensing layer A) PT-COOH, B) PT-COOR, C) P3HT, D) PQT12 under ambient exposure condition, including no light exposure. 25 consecutive scans were applied in order to analyze magnitude of drift nature and direction. Output characteristic for polymer sensing layer E) PT-COOH, F) PT-COOR, G) P3HT, H) PQT12 with ambient exposure condition, including no light exposure. An applied gate voltage of -50 V was set.

Figure 2. Output characteristic for polymer sensing layer A) PT-COOH, B) PT-COOR, C) P3HT, D) PQT12 with continuous exposure to various concentrations of NO₂ for 3 minutes before each consecutive measurement with an applied V_g = -50 V. Transfer characteristic for polymer sensing layer E) PT-COOH, F) PT-COOR, G) P3HT, H) PQT12 with exposure to various concentrations of NO₂ for 3 minutes before each consecutive measurement.

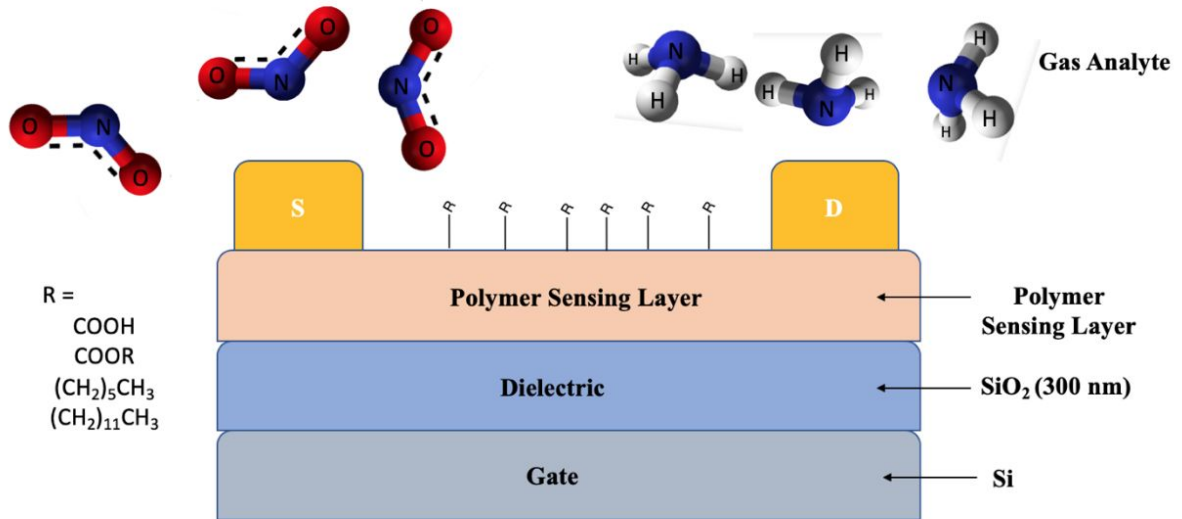
Figure 3. Output characteristic for polymer sensing layer A) PT-COOH, B) PT-COOR, C) P3HT, D) PQT12 with continuous exposure to various concentrations of NH₃ for 3 minutes before each consecutive measurement with an applied V_g = -50 V. Transfer characteristic for polymer sensing layer E) PT-COOH, F) PT-COOR, G) P3HT, H) PQT12 with exposure to various concentrations of NH₃ for 3 minutes before each consecutive measurement.

Figure 4. Sensitivity Response of each polymer sensing layer with exposure to various concentrations of A) NO₂ and B) NH₃ for 3 minutes before each consecutive measurement. Represents a continuous flow exposure analysis where a device is subjected to each concentration for 3 minutes, measured, and re-subjected to another higher concentration. This was repeated and averaged with at least 4 devices.

Figure 5. Transfer Curves of remote-gate field effect transistor A) PT-COOH, B) PT-COOR, C) P3HT, and D) PQT12 with NO₂ Exposure for 20 minutes at 1 ppm and 20 ppm with recovery obtained at 60°C in vacuum for 1 hour. Acetonitrile was used as the contact solvent between extended gate and remote gate field effect transistor. V_{TH} analysis of each polymer sensing layer E) PT-COOH, F) PT-COOR, G) P3HT, H) PQT12 with exposure to NO₂ (1 ppm, 20 ppm, and Recovery) and NH₃ (1 ppm and 20 ppm) using ACN as contact solvent. Segment Measurements pertains to 20 consecutive scans that are averaged with 4 sample trials of each sample measurement. Associates with drift analysis before restoration is reached.

Figure 6. A) Hole concentrations of polymer sensing layer before and after 1 ppm exposure of NO₂ due to calculating the voltage shift occurrence with the incorporation of the RG FET platform. Initial hole concentration was obtained from μ_h from OFET using transfer curve

and conductivity (σ). B) Mobility for unexposed devices was obtained from FET measurements, while mobility for NO_2 -exposed devices was calculated based on hole concentrations obtained by using $\sigma = e \cdot \mu_h \cdot p_0$. C) Conductivity measurement of polymer sensing layer before and after 1 ppm NO_2 and NH_3 exposure.



Scheme 1

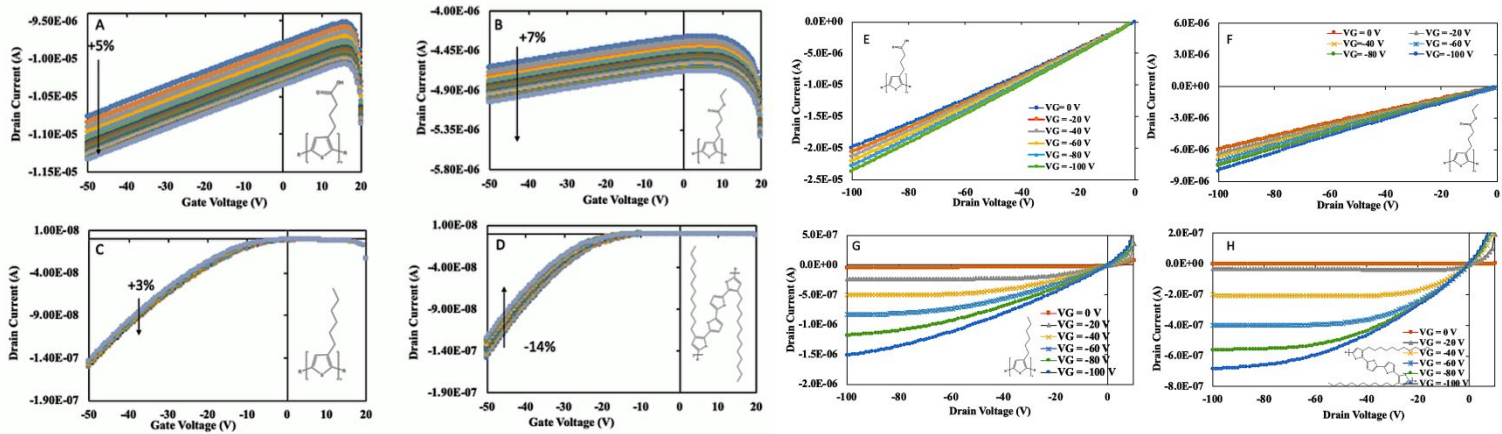


Figure 1

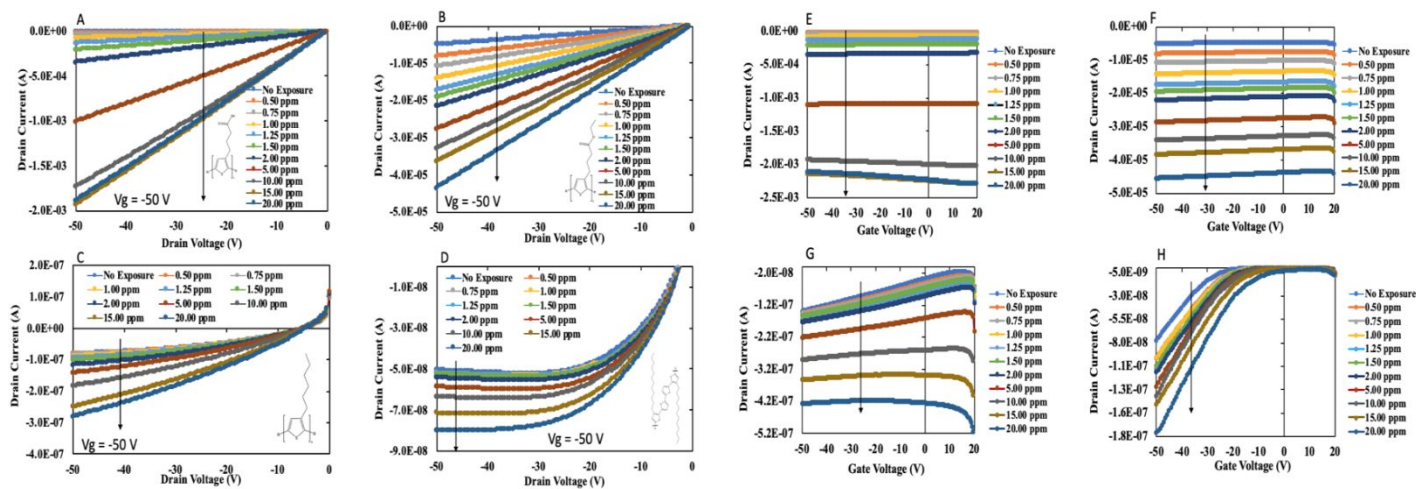


Figure 2

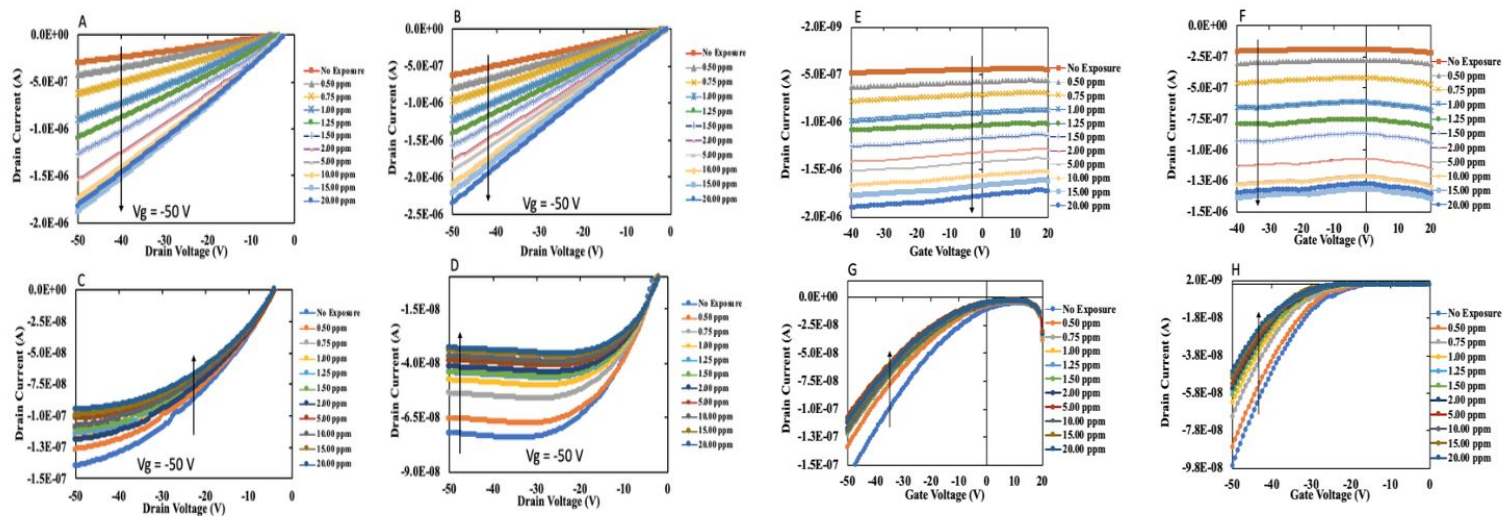


Figure 3

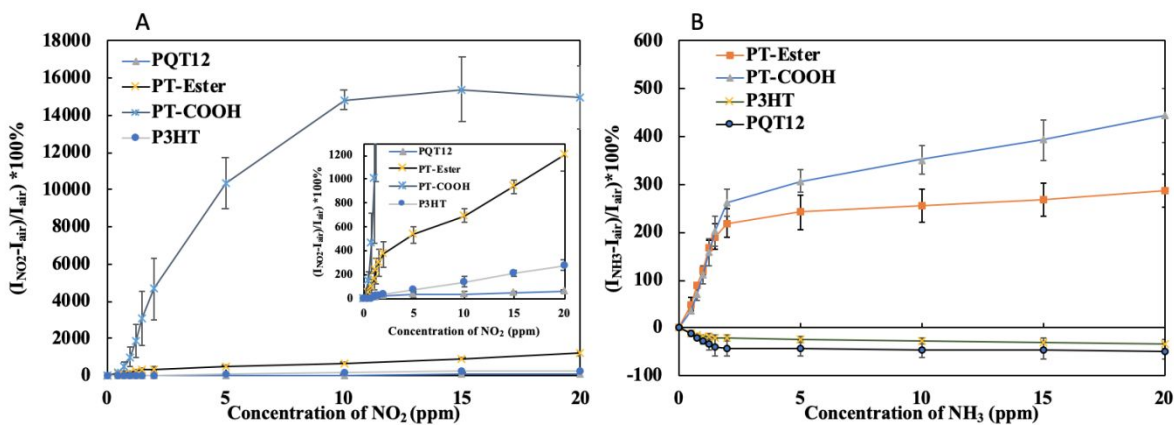


Figure 4

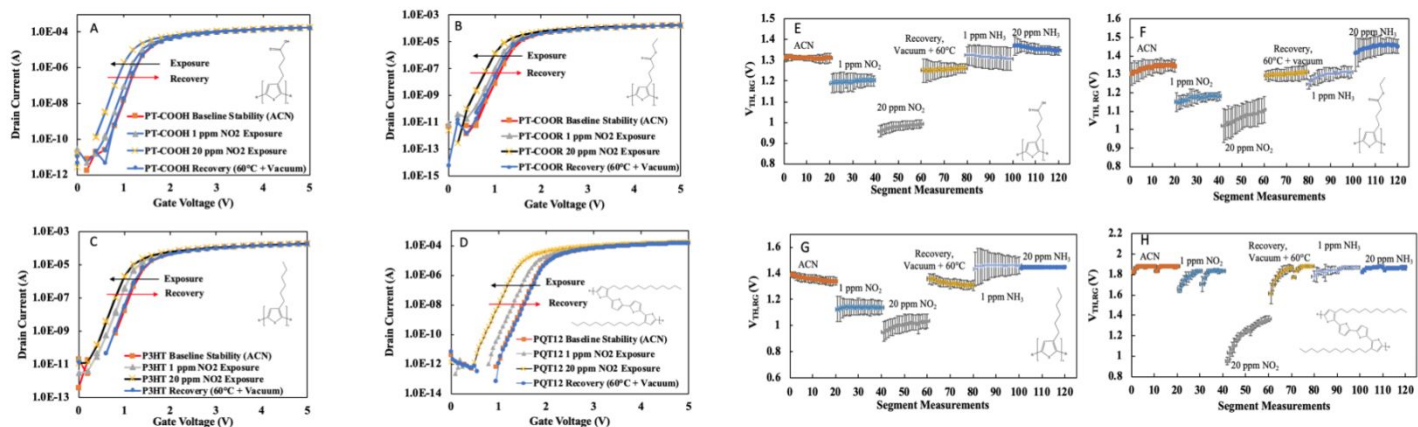


Figure 5

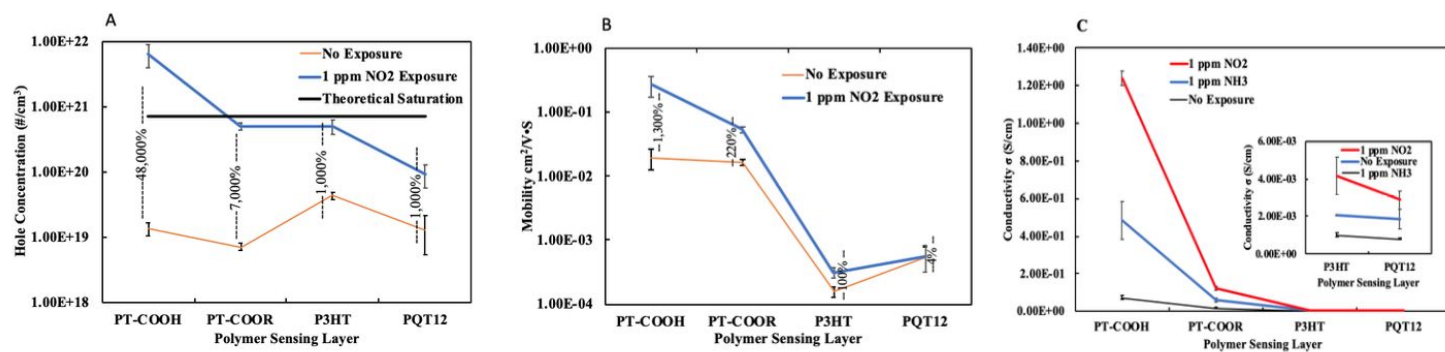


Figure 6